Hindawi
International Transactions on Electrical Energy Systems
Volume 2022, Article ID 6396345, 13 pages
https://doi.org/10.1155/2022/6396345

Research Article

A Novel Coordinated Control System to Reactive Power Compensation of Photovoltaic Inverter Clusters

Tingzhe Pan [1,2]

[1]*China Southern Power Grid Electric Power Research Institute Co., Ltd, Guangzhou, China*
[2]*Guangdong Provincial Key Laboratory of Intelligent Measurement and Advanced Metering of Power Grid, Guangzhou, China*

Correspondence should be addressed to Tingzhe Pan; 18900220639@163.com

Received 21 February 2022; Revised 30 August 2022; Accepted 9 September 2022; Published 11 October 2022

Academic Editor: Pawan Sharma

With the development of new energy, a cost-effective reactive power compensation scheme is essential to the voltage stability of the power system for small-capacity distributed generation. This paper proposes a coordinated control scheme of inverter cluster which is based on the reactive power support capability of the photovoltaic inverter. Moreover, by using power angle vectors, a reactive power distribution algorithm is proposed to solve the poor power quality of the point of common coupling connecting source and load in the distributed generation station. Simulations verify the performance of the algorithm is better than the conventional static capacity distribute algorithm and dynamic residual margin distribute algorithm. Finally, the effectiveness of the reactive power compensation scheme and distribution strategy for improving power quality and regulation ability proposed in this paper is verified by operation experiments in the actual power station.

1. Introduction

With the increasing urgency to protect the environment and the deepening of government energy reform, renewable energy such as photovoltaic (PV) and wind power will join in the grid on a large scale in the next few years and gradually replace the traditional power generation to dominate future energy supply. Small-capacity distributed PV cobuilt with factories and buildings is widely adopted for development because of its low construction cost, flexible grid control, and rich construction sites. Distributed and small-capacity PV stations will be a crucial part of the future grid [1–5].

As a power generation unit, the inverter is the key equipment of PV power stations (PVPS). With the development of electronics technology, the inverter is evolving in the direction of digitization, intelligence, and multifunction. PV inverters can achieve separate control of active and reactive power through decoupling and have the ability to undertake the power grid frequency and voltage regulation [6–13]. Meanwhile, with the development of digital technology, the control accuracy, conversion efficiency, and response speed of PV inverter will gradually be better than the traditional generator and feeder equipment [14–16].

Renewable generation has significant randomness and volatility, so unregulated pure active power output has a major impact on power quality and system stability [12, 17]. Dynamic reactive power control can compensate the system voltage and power factor (PF) in real time, and the traditional way is to configure Static Var Generator (SVG) at the point of common coupling (PCC) of PVPS [18, 19]. However, for small-capacity distributed generation (DG) stations, SVG is expensive and inefficient.

Applying inverters to compensate the reactive power while generating energy can achieve the same effect as SVG and can stabilize the feeder voltage and reduce line losses [20–22]. It is a current research hotspot to coordinate and control individual small-capacity inverter groups to achieve the overall superior system performance of PVPS. At present, the industry has proposed a variety of control algorithms for volt/var control (VVC) and has achieved certain results in closed-loop simulation and local experiments [3, 6]. Through sorting and comparison of different

Table 1: VCC algorithm comparison description.

Reactive power compensation program of PVPS	Advantages	Disadvantages

Compensate with SVG/SVC at PCC	Response speed (+++++);
	power quality at PCC (+++++);
	simple control (+++);
	night compensation;
		High investment costs (+);
		large power consumption (+);
		damage rate (+);
		no station topology optimization (+);

Compensate with SVG/SVC at distributed generation node and internal confluence point	Response speed (+++);
	power quality at PCC (+++);
	station topology optimization (++ reduce line loss and improve stability margin);
		Complex control (++);
		no night compensation;
		high investment costs (++);
		large power consumption (++);
		damage rate (++);

Compensate with SVG/SVC at PCC and inverters at distributed generation node	Response speed (++++);
	power quality at PCC (++++);
	night compensation;
	station topology optimization (++)
		Complex control (++);
		high investment costs (++);
		large power consumption (++);
		damage rate (+);

Compensate with inverters actively by embedding PVPS model at generation node	Response speed (+++++);
	no investment costs (+++);
	no power consumption (+++);
	damage rate (+++);
	station topology optimization (+++)
		Power quality at PCC (+ oscillation caused by over compensation);
		complex control (+);
		no night compensation;

Compensate with inverters by static allocation of station control system at generation node	Power quality at PCC (++);
	no investment costs (++++);
	no power consumption (+++);
	damage rate (+++);
	station topology optimization (+++);
		Response speed (+);
		complex control (++);
		no night compensation;

Compensate with inverters by dynamic intelligent distribution of station control system at generation node	Power quality at PCC (+++);
	no investment costs (++++);
	no power consumption (+++);
	damage rate (+++);
	station topology optimization (++++);
		Response speed (++);
		complex control (+);
		no night compensation;

(*better performance with more +).

VCC algorithms, as shown in Table 1, the problems and research progress motivate the current research work of this paper [23–29].

As a distributed group topology, how to allocate each inverter in different states involves active power generation, voltage balance, and compensation effect, which is the key step of using the inverter as the main reactive power source [26, 27]. However, as shown in Table 1, the existing applications mostly consider how to ensure the compensation effect and PVPS revenue, while ignoring the equilibrium problem of DG nodes [30, 31]. And algorithms are mostly based on simulation analysis, ignoring the interference to the environment and sampling data, as well as experimental verification and engineering applications sometimes [32]. Based on this, this paper proposes an algorithm for reactive power equilibrium distribution of parallel devices, which can provide a solution to the existing problems.

The technical scheme of using DG devices for system reactive power compensation (RPC) is considered in this paper to reduce the investment cost. On the premise of ensuring the overall compensation effect, an angle length distributed algorithm for the distributed confluence device based on the power angle vector relationship is proposed, to reduce the difference between different devices and improve the system stability. On the other hand, two other low data dimension inverter group reactive power distribution (RPD) algorithms are compared and analyzed, and the effects of different algorithms on voltage equalization and maximum compensation capability are summarized. Simulation results verify the effectiveness of the proposed study. Finally, the angle length distribution algorithm is embedded into the PVPS control system for operation experiments. The long-term operation results prove the feasibility of the technical route and distribution strategy in this paper, which provides an effective and balanced idea of RPC for distributed PVPS.

2. Power Model

Due to the shortage of land resources and high investment costs, the construction process of centralized high-voltage PVPS slows down. With the opening of China's PV grid connection policy and the reduction of PV module cost, increasingly factories and buildings participate in the construction of distributed PV to save electricity costs and participate in power market transactions. The topology of distributed PVPS is shown in Figure 1. The power station and load converge at PCC and are jointly subject to the grid power quality assessment [28]. Different PV matrices in the station are converged in PCC_{PV} through transformers. Each PV matrix is composed of different numbers of inverters and PV arrays. Thus, the PVPS is a multigeneration node grouping and hierarchical converging system [32].

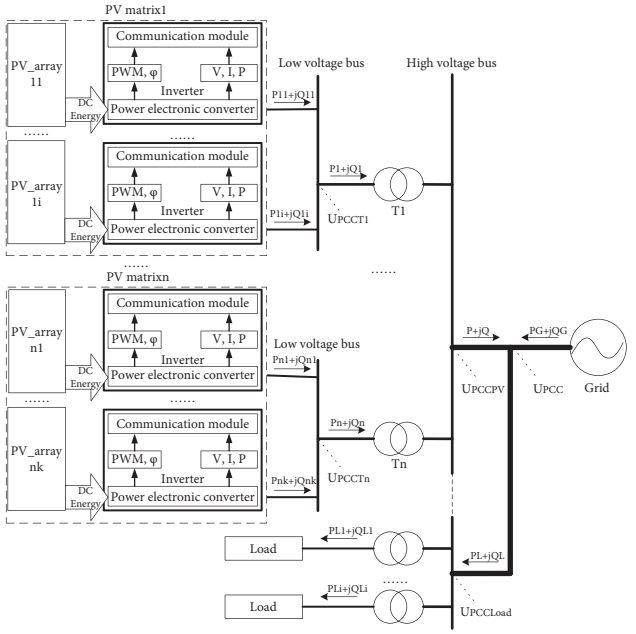

Figure 1: Topology of distributed PVPS.

PV inverter usually operates at a constant PF (usually 1) to improve power generation, which leads to uncontrollable reactive power with the change of light and temperature [12, 22]. Figure 2 shows the statistical status of Hisense PVPS in Foshan, China, with inverters at 0.95 fixed PF running within a week, and the phenomenon that the power station generates electricity with relatively stable PF in PCC_{PV} during the generation period can be seen from the figure. With the periodic increase of power generation at noon every day, the active and reactive power transmitted by PVPS to the high-voltage bus will also undergo periodic changes. Due to the randomness and volatility of PV power generation, this feature does not have a quantifiable law.

The influence of reactance of the transmission line between PCC_{PV}, PCC, and PCC_{Load} is ignored in the topology of Figure 1 [28], so formula (1) is satisfied.

Under the fixed PF mode, P and Q of PVPS change at the same time at PCC_{PV}, assuming that the load remains unchanged, so the power fluctuation caused by PV will be reflected in the grid, resulting in dramatic changes in Figure 2, especially the fluctuation of active power. This behavior, which does not consider dynamic RPC but only pursues the generation efficiency and fixed operation mode, has caused a serious burden to the power system. With the continuous construction and development of PV industry, as well as the increasing popularity of power substitution and power consumption upgrading, this burden will become more severe in the increasingly high penetration power system. Meanwhile, the continuous bad PF at PCC will cause assessment fines to users [22].

$$\begin{cases} P_G = P_L - P, \\ Q_G = Q_L - Q. \end{cases} \tag{1}$$

3. Algorithm

PV inverter can realize the decoupling control of active power and reactive power [7, 11, 12]. The control logic of RPC designing with this paper is shown in Figure 3 [22]. According to the comprehensive status of power quality obtained at PCC, the reactive power ΔQ needing to be regulated is calculated, and then, the reactive power execution of the inverter is obtained through the feeder distribution algorithm and the inverter group distribution algorithm, as well as the power iteration between groups [32]. The scheme in Figure 3 is a dynamic real-time tracking control [28], so the oscillation amplitude of the control effect is related to the interval period between two commands. Assuming that the normally control oscillation will not exceed the system limits, and the safety threshold is set at PCC, the stabilization device will be started when the disturbance exceeds the system requirements. Meanwhile, the inverter is also embedded with the regulation threshold and voltage operation limit in each one to ensure to resist the disturbance during the real-time operation quickly. As the control system of PVPS is very complex and includes LVRT and HVRT, other reconstruction works will not be described in detail in this paper. In short, the RPC effect will eventually converge in the real-time correction control mode.

RPD algorithm is related to the overall compensation effect of the inverter as the reactive power source and the balance between different matrices and inverters. This chapter compares and analyzes the compensation ability, operation balance, and stability control ability of three different algorithms.

3.1. Ratio Distribute Algorithm. Transformers and inverters have independent static parameters to adapt to the complex field environment. Taking the device capacity as an allocation basis, the static distribution algorithm is designed as shown in Table2. Algorithm 1 does not consider the dynamic operation parameters of devices. Although RPC quantity ΔQ reflects part of the dynamic parameters, the fixed allocation ratio does not play a sufficient role in compensating and balancing when the dynamic parameters of the device group differ greatly, which wastes the group control effect.

The topology of PVPS and the parameters of each device shown in this paper are based on the Foshan Hisense distributed PVPS in China. Define the topology of Figure 1 with 5 PV matrixes converging at PCC_{PV}, and [14 13 15 15 15] PV arrays converging at PCC_{Ti} separately. Table 3 shows the static capacity parameters of each device, and Table 4 defines the dynamic operation parameters under three typical cases.

The relationship between the demand of RPC amount $\Delta Q \in [0, C]$ and the actual distribution value meets Formula (2), which is the capacity constraint.

$$\sum_{k=1}^{k=m} \Delta QT(k) = \sum_{k=1}^{k=m} \sum_{j=1}^{j=n} \Delta QI_k(j) \le \Delta Q. \tag{2}$$

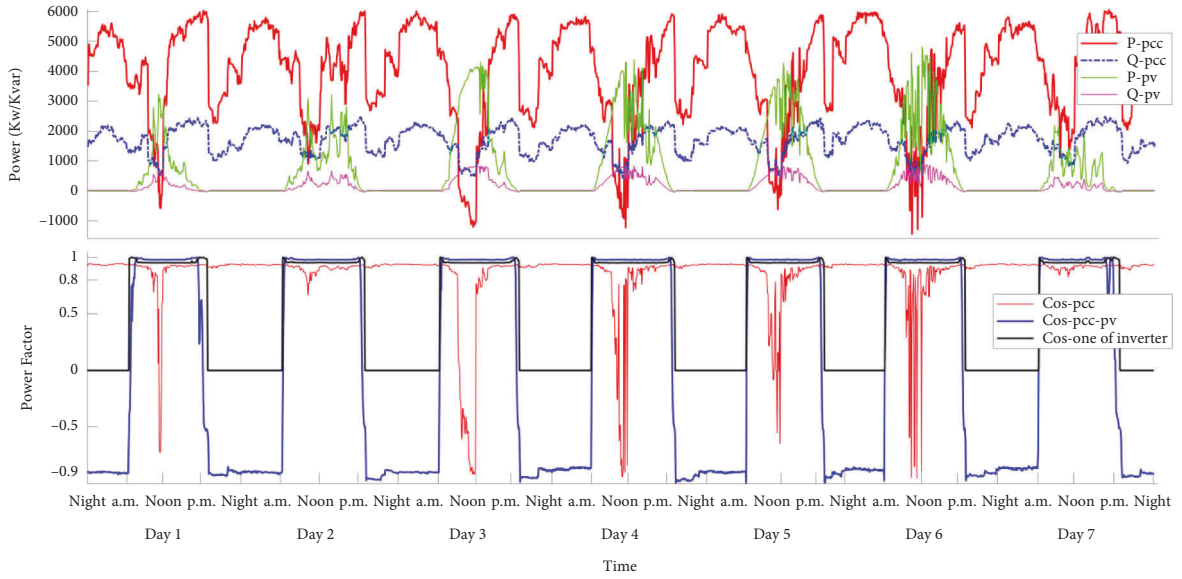

Figure 2: PF comparison diagram of PVPS without compensation.

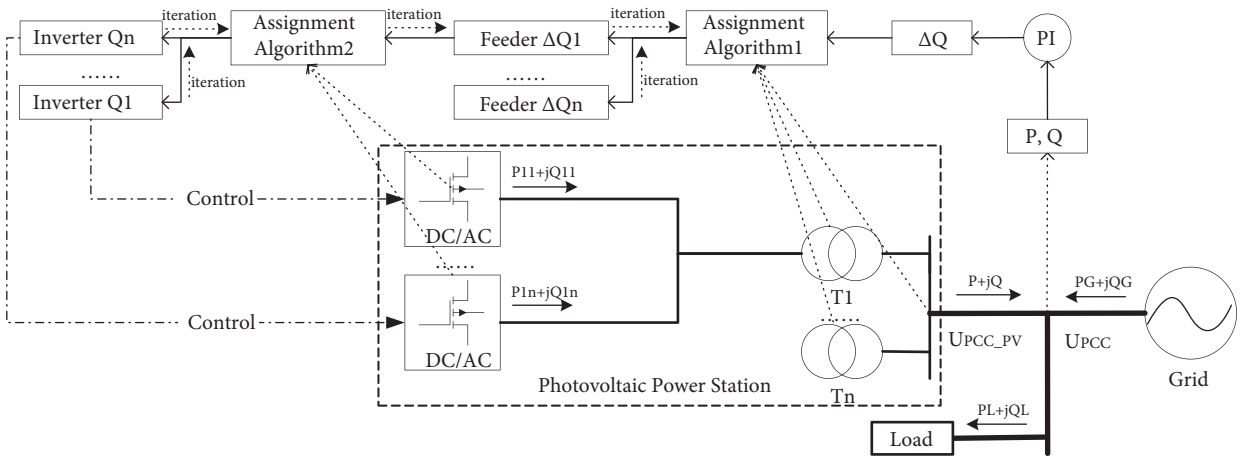

Figure 3: RPC control logic of PVPS.

Table 2: Ratio distribute algorithm of static capacity.

Algorithm 1: Ratio distribute algorithm
Input: RPC amount ΔQ; transformer capacity matrix CT; inverter capacity matrix CI;
Output: transformer reactive power adjustment matrix ΔQT; inverter reactive power adjustment matrix ΔQI;
(1): Initialize, arrange CT according to the sequence of transformer grid connection, the length of CT is m , make $k = 1$;
(2): Repeat
(3): Calculate $\Delta QT(k) = (\Delta Q - \sum_{i=1}^{k-1} \Delta QT(i)) \times CT(k) / \sum_{i=k}^{m} CT(i)$, among which $k = 1$, $\Delta QT(1) = \Delta Q \times CT(1) / \sum_{i=1}^{m} CT(i)$;
(4): Initialize inverter group under transformer feeder, $CI_k = f(CI)$, $\Delta QI_k =$, $j = 1$;
(5): Repeat
(6): Calculate $\Delta QI_k(j) = (\Delta QT(k) - \sum_{i=1}^{j-1} \Delta QI_k(i)) \times CI_k(j) / \sum_{i=j}^{n} CI_k(i)$, among which $j = 1$, $\Delta QI_k(1) = \Delta QT(k) \times CI_k(1) / \sum_{i=1}^{n} CI_k(i)$;
(7): Update $j = j + 1$;
(8): Until $j = n$ in CI_k;
(9): Update $\Delta QT(k) = \sum_{i=1}^{n} \Delta QI_k(i)$, verify the constraints of formula (2);
(10): Update $k = k + 1$;
(11): Until $k = m$ in CT;

Table 3: Static parameters of PVPS installation.

Parameter	Static value (rated capacity)/(kW)
Transformer	[1000 800 1250 1250 1250]
PV matrix 1	[50 80 80 80 80 80 80 50 80 80 80 80 50 50]
PV matrix 2	[80 80 80 80 50 50 50 50 80 50 80 50 50]
PV matrix 3	[80 80 80 80 80 80 80 80 80 80 80 80 80 80 80]
PV matrix 4	[80 80 80 80 80 80 80 80 80 80 80 80 80 80 80]
PV matrix 5	[80 80 80 80 80 80 80 80 80 80 80 80 80 80 80]

Table 4: Dynamic parameters of PVPS installation.

Parameter		Dynamic value/(kW)		
		Case 1	Case 2	Case 3
Transformer	Active power	All 0	[500 400 625 625 625]	[900 720 1125 1125 1125]
	Reactive power	All 0	[500 400 625 625 625]	All 0
PV matrix 1	Active power	All 0	[25 40 40 40 40 40 40 25 40 40 40 40 25 25]	[45 72 72 72 72 72 72 45 72 72 72 72 45 45]
	Reactive power	All 0	[25 40 40 40 40 40 40 25 40 40 40 40 25 25]	All 0
PV matrix 2	Active power	All 0	[40 40 40 40 25 25 25 25 40 25 40 25 25]	[72 72 72 72 45 45 45 45 72 45 72 45 45]
	Reactive power	All 0	[40 40 40 40 25 25 25 25 40 25 40 25 25]	All 0
PV matrix 3	Active power	All 0	[40 40 40 40 40 40 40 40 40 40 40 40 40 40 40]	[72 72 72 72 72 72 72 72 72 72 72 72 72 72 72]
	Reactive power	All 0	[40 40 40 40 40 40 40 40 40 40 40 40 40 40 40]	All 0
PV matrix 4	Active power	All 0	[40 40 40 40 40 40 40 40 40 40 40 40 40 40 40]	[72 72 72 72 72 72 72 72 72 72 72 72 72 72 72]
	Reactive power	All 0	[40 40 40 40 40 40 40 40 40 40 40 40 40 40 40]	All 0
PV matrix 5	Active power	All 0	[40 40 40 40 40 40 40 40 40 40 40 40 40 40 40]	[72 72 72 72 72 72 72 72 72 72 72 72 72 72 72]

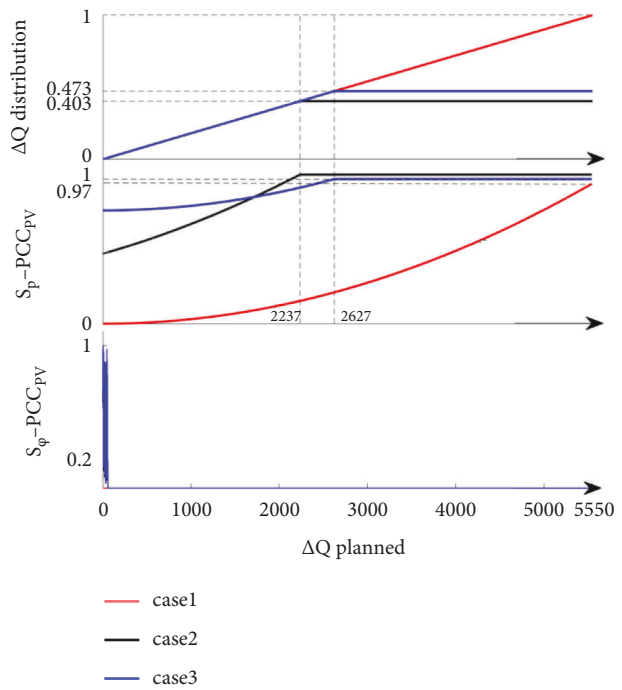

Figure 4: The results of algorithm 1 for the case.

The greater the difference in the operation state of feeder devices, the more obvious the imbalance of the station system, and the phenomenon of voltage imbalance and power backflow after confluence is more serious. Therefore, the difference of feeder array under the same PCC is an important index to measure the merits and disadvantages of

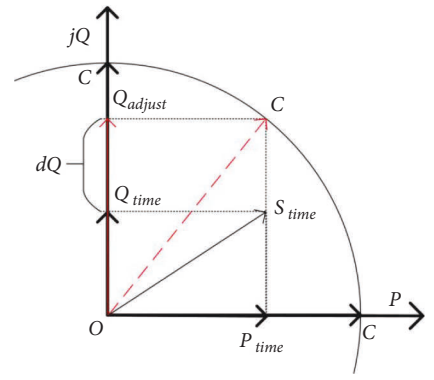

Figure 5: RPC power vector diagram.

the RPD algorithm. This paper defines the phase difference and power difference as Formulas (3) and (4), where φ is the phase angle, and SS is the apparent power of one device.

$$s_\varphi = \frac{\sum_{i=1}^{n} (\varphi_i - \overline{\varphi})^2}{n}. \tag{3}$$

$$s_P = \frac{\sum_{i=1}^{n} (S_i - \overline{S})^2}{n}. \tag{4}$$

Algorithms in this paper are all implemented in MATLAB 2021a, and the PVPS model in Figure 1 is built to calculate the cases in the above table, and the normalized result is shown in Figure 4.

Since the initial power state of each device in Case 2 and Case 3 is not 0, the reactive power that can be allocated will reach saturation earlier, and the corresponding power

Table 5: Residual margin algorithm of one-dimensional dynamic capacity.

Algorithm 2: Residual margin algorithm
Input: RPC amount ΔQ; transformer capacity matrix CT, transformer real-time active power matrix PT, transformer real-time reactive power matrix QT; inverter capacity matrix CI, inverter real-time active power matrix PI, inverter real-time reactive power matrix QI;
Output: transformer reactive power adjustment matrix ΔQT; inverter reactive power adjustment matrix ΔQT;
(1): Initialize, arrange CT according to the sequence of transformer grid connection, the length of CT is m, make $k = 1$;
(2): Calculate reactive power margin matrix of transformer dQT by formula (5);
(3): Repeat
(4): Calculate $\Delta QT(k) = (\Delta Q - \sum_{i=1}^{k-1} \Delta QT(i)) \times dQT(k) / \sum_{i=k}^{m} dQT(i)$, among which $k = 1$, $\Delta QT(1) = \Delta Q \times dQT(1) / \sum_{i=1}^{m} dQT(i)$;
(5): Initialize inverter group under transformer feeder, $\Delta QI_k =$, $j = 1$, calculate reactive power margin matrix of inverter dQI_k by formula (5);
(6): Repeat
(7): Calculate $\Delta QI_k(j) = (\Delta QT(k) - \sum_{i=1}^{j-1} \Delta QI_k(i)) \times dQI_k(j) / \sum_{i=j}^{n} dQI_k(i)$, among which $j = 1$, $\Delta QI_k(1) = \Delta QT(k) \times dQI_k(1) / \sum_{i=1}^{n} dQI_k(i)$;
(8): Update $j = j + 1$;
(9): Until $j = n$ in dQI_k;
(10): Update $\Delta QT(k) = \sum_{i=1}^{n} \Delta QI_k(i)$, verify the constraints of formula (2);
(11): Update $k = k + 1$;
(12): Until $k = m$ in CT;

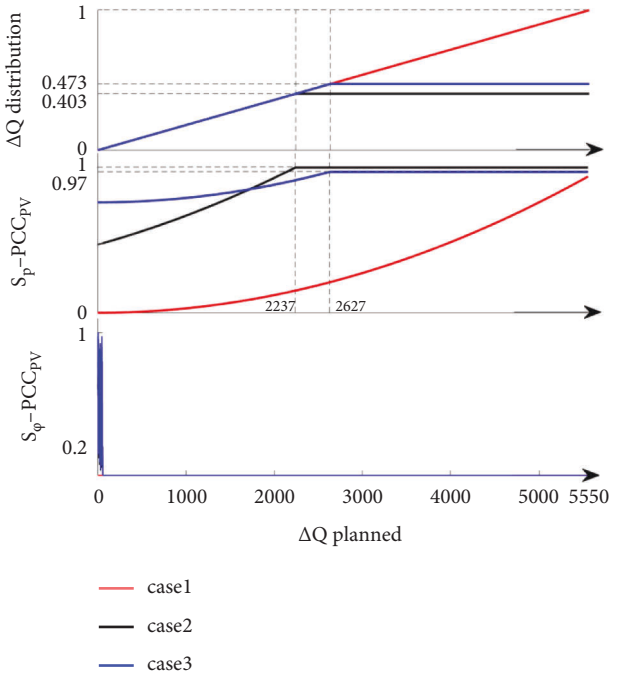

Figure 6: The results of algorithm 2 for the case.

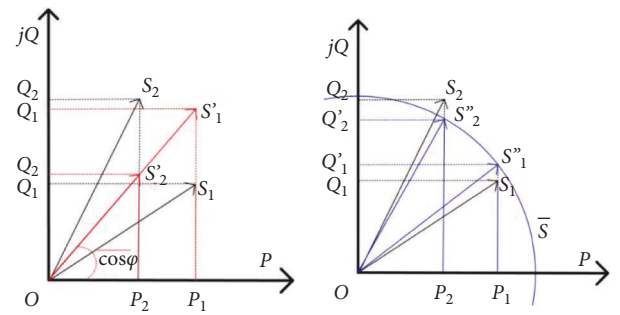

Figure 7: Reactive power adjustment under average angle and length of power. (a) Vector diagram of average angle. (b) Vector diagram of average length.

difference remains unchanged after saturation, while the power difference in Case 1 continues to increase steadily. The phase difference in Case 2 and Case 3 is larger when the planned ΔQ is small, but when the planned ΔQ is increased to compensate for the initial value difference enough, the phase difference remains at 0.

3.2. Residual Margin Algorithm. Define the dynamic parameters of remaining capacity dQ when the inverter is running, as shown in Figure 5. In most cases, the inverters are in state S_{time}, and the maximum additional RPC dQ can be provided without loss of generating power P_{time}, as formula (5), where C is the apparent power of the inverter. Taking dQ as the allocation basis, a one-dimensional dynamic distribution algorithm is designed as shown in Table 5.

Calculate the cases in Tables 3 and 4 through Algorithm 2, and the normalized result is shown in Figure 6. By observing the trend of Figures 4 and 6, the optimization results of Algorithm 2 and Algorithm 1 are basically consistent.

$$dQ = \sqrt{C^2 - P_{time}^2 - Q_{time}}. \quad (5)$$

3.3. Angle Length Distribute Algorithm. In this section, the distribution principle is based on the imbalance degree without considering the power margin. In each RPD, the difference in PF and apparent power between the devices connected at PCC and the lower level is considered to balance the phase angle and power amplitude of different devices.

Figure 7(a) shows that two devices under one PCC achieve the same PF $\overline{\cos\varphi}$ by adjusting the reactive power. This adjustment does not change the active power

Table 6: Angle length distributed algorithm of multidimensional dynamic capacity.

Algorithm 3: Angle length distributed algorithm
Input: RPC amount ΔQ; transformer capacity matrix CT, transformer real-time active power matrix PT, transformer real-time reactive power matrix QT; inverter capacity matrix CI, inverter real-time active power matrix PI, inverter real-time reactive power matrix QI;
Output: transformer reactive power adjustment matrix ΔQT; inverter reactive power adjustment matrix ΔQT;
(1): Initialize, arrange CT according to the sequence of transformer grid connection, the length of CT is m, make $k = 1$;
(2): Repeat
(3): Calculate average PF matrix of transformer $\overline{\cos\varphi T_k}$ by formula (6);
(4): Calculate apparent power matrix of transformer $\overline{ST_k}$ by formula (7);
(5): Calculate $\Delta QT_\varphi(k) = \sqrt{(1-\overline{\cos\varphi T_k}^2)}/\overline{\cos\varphi T_k} \times PT(k) - QT(k)$;
(6): Calculate $\Delta QT_s(k) = \sqrt{\overline{ST_k}^2 - PT(k)^2 - QT(k)}$;
(7): Then calculate $\Delta QT(k) = \Delta QT_s(k) + \Delta QT_\varphi(k)/2$;
(8): Initialize inverter group under transformer feeder, $\Delta QI_k =$, $j = 1$;
(9): Repeat
(10): Calculate average PF matrix of inverter $\overline{\cos\varphi I_{kj}}$ by formula (6);
(11): Calculate apparent power matrix of inverter $\overline{SI_{kj}}$ by formula (7);
(12): Calculate $\Delta QI_{k\varphi}(j) = \sqrt{(1-\overline{\cos\varphi I_{kj}}^2)}/\overline{\cos\varphi I_{kj}} \times PI_k(j) - QI_k(j)$;
(13): Calculate $\Delta QI_{ks}(j) = \sqrt{\overline{SI_{kj}}^2 - PI_k(j)^2 - QI_k(j)}$;
(14): Then calculate $\Delta QI_k(j) = \Delta QI_{k\varphi}(j) + \Delta QI_{ks}(j)/2$;
(15): Update $j = j + 1$;
(16): Until $j = n$ in CI_k;
(17): Update $\Delta QT(k) = \sum_{i=1}^{n} \Delta QI_k(i)$, verify the constraints of formula (2);
(18): Update $k = k + 1$;
(19): Until $k = m$ in CT;

generation P_1P_1 and P_1P_2 and ensures the stability of total reactive power: $Q_1 + Q_2 = Q_1' + Q_2'$. Due to the large number of devices connected to the PCC, the approximate solution of Formula (6) is adopted for the average PF.

$$\begin{cases} \overline{\cos\varphi_j} = \dfrac{\sum_{i=j}^{n} P(i)}{\sqrt{\left(\sum_{i=j}^{n} P(i)\right)^2 + \left(\sum_{i=j}^{n} Q(i) + \Delta Q - \sum_{i=1}^{j-1}\Delta Q_i\right)^2}}, j > 1, \overline{\cos\varphi_1} = \dfrac{\sum_{i=1}^{n} P(i)}{\sqrt{\left(\sum_{i=1}^{n} P(i)\right)^2 \left(\sum_{i=1}^{n} Q(i) + \Delta Q\right)^2}}, j = 1. \end{cases} \tag{6}$$

Figure 7(b) shows that two devices under one PCC achieve the same apparent power $\overline{S}$ by adjusting the reactive power. This adjustment will also guarantee the active power generation and the total reactive power: $Q_1 + Q_2 = Q_1'' + Q_2''$, and the average apparent power is calculated by the approximate solution of Formula (7).

$$\begin{cases} \overline{S_j} = \sqrt{\left(\sum_{i=j}^{n} P(i)\right)^2 + \left(\sum_{i=j}^{n} Q(i) + \Delta Q - \sum_{i=1}^{j-1}\Delta Q_i\right)^2 \times \dfrac{C(j)}{\sum_{i=j}^{n} C(i)}}, j > 1, \overline{S_1} = \sqrt{\left(\sum_{i=1}^{n} P(i)\right)^2 + \left(\sum_{i=1}^{n} Q(i) + \Delta Q\right)^2 \times \dfrac{C(1)}{\sum_{i=1}^{n} C(i)}}, j = 1. \end{cases} \tag{7}$$

From Figure 7 and Formulas (6) and (7), it can be seen that the angle average or length average reduces the difference between devices in different dimensions, which is conducive to the power convergence of the device group, and reduces the system stability impact caused by the differential fluctuation of distributed nodes. Based on this, the designed algorithm is shown in Table 6.

Maintain the same environment as Algorithm 1 and Algorithm 2, and simulate Algorithm 3. The normalized result is shown in Figure 8. It can be seen from the results

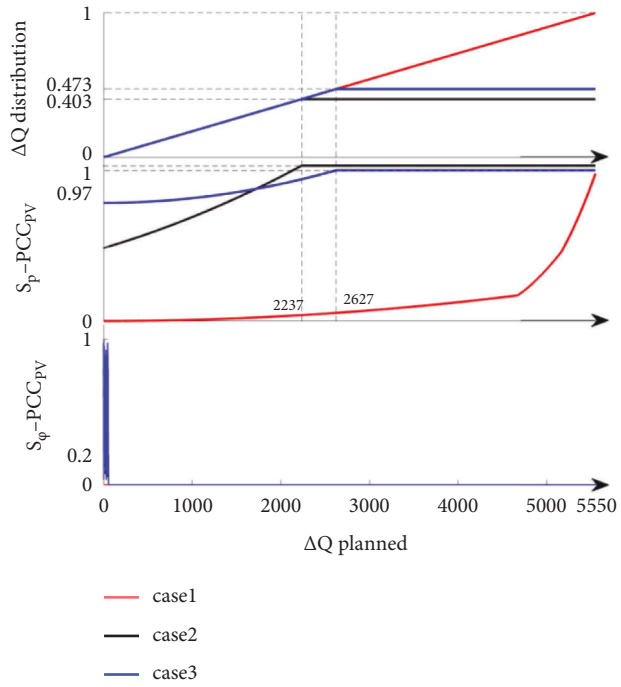

Figure 8: The results of algorithm 3 for the case.

Table 7: Comparison and description of algorithms this paper.

Algorithm	Advantages	Disadvantages
Ratio distribute algorithm	Simple control (+++)	RPC capability (+ ΔQ) stability margin (+) balance ability (+ s_p)
Residual margin algorithm	Balance ability (++ s_p)	Complex control (++) RPC capability (+ ΔQ) stability margin (+)
Angle length distributed algorithm	RPC capability (++ ΔQ) stability margin (++) balance ability (+++ s_p)	Complex control (+)

(*better performance with more +).

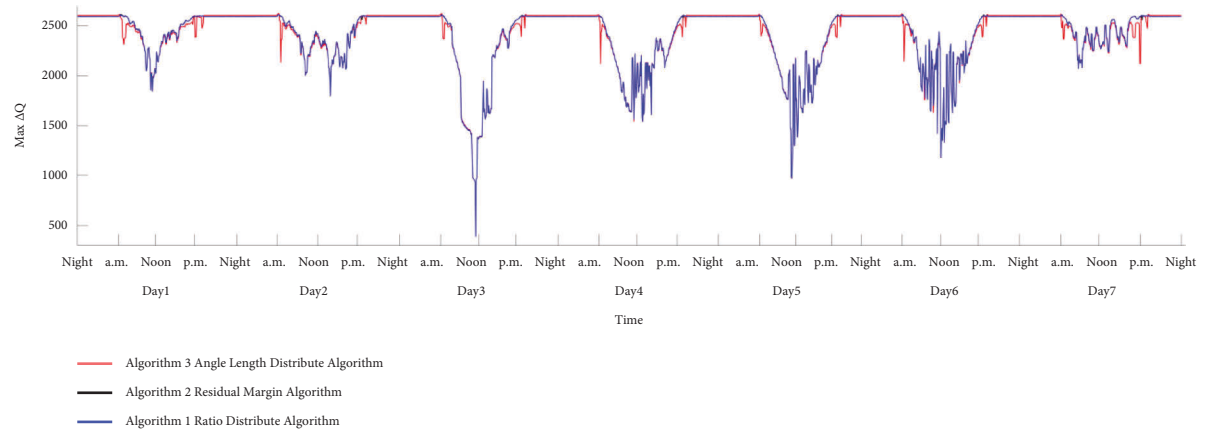

Figure 9: Maximum ΔQ comparison of three algorithms.

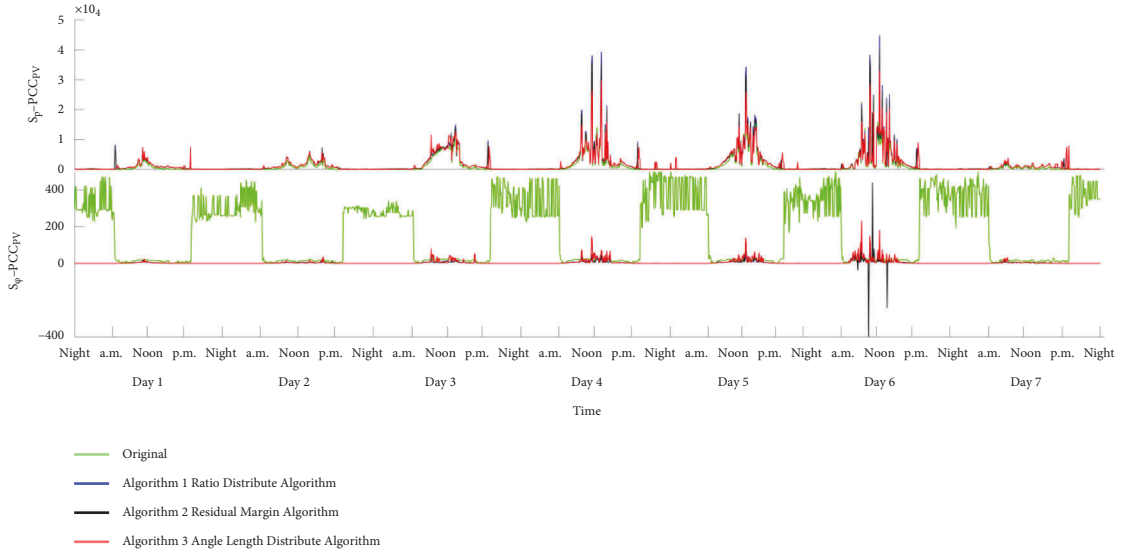

Figure 10: Transformer difference comparison of three algorithms in PCC_{PV}.

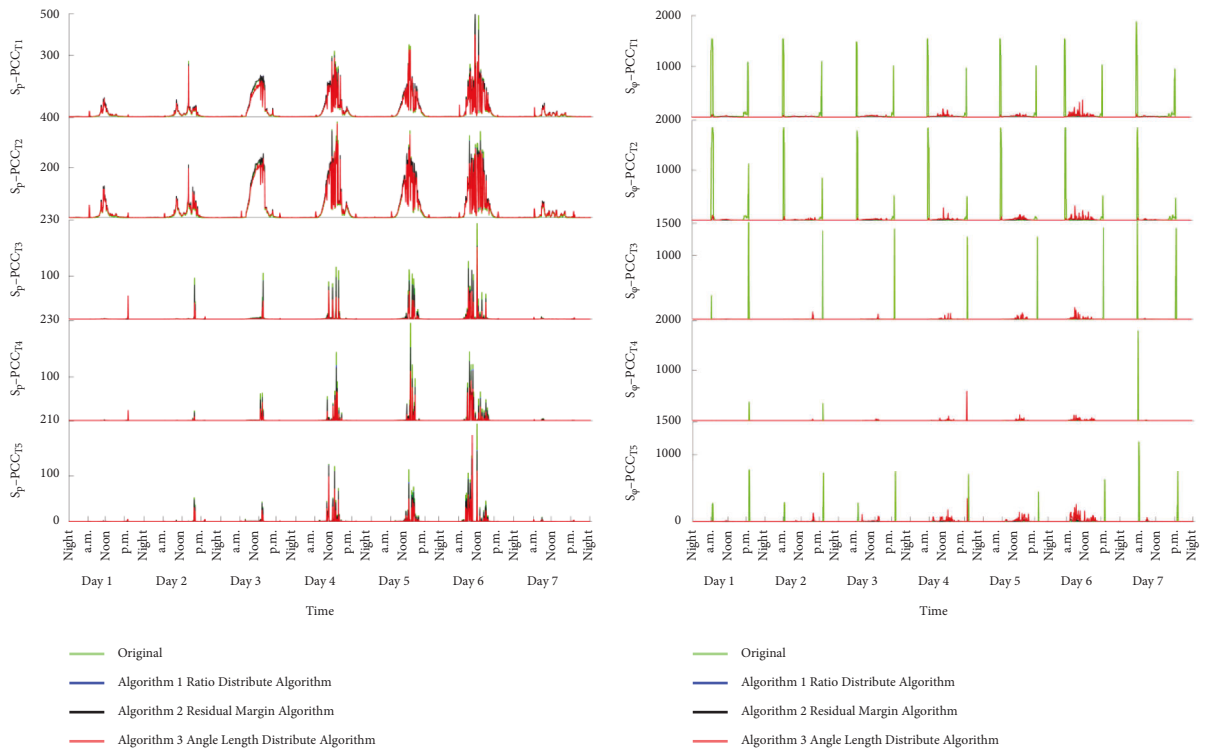

Figure 11: Inverter array difference comparison of three algorithms in PCC_{Ti}.

that Algorithm 3 is significantly better than the first two algorithms in terms of power imbalance in Case 1, and the power imbalance degree keeps a very low growth rate in most of the planned ΔQΔQ, but the overall change law still remains consistent.

3.4. Comparison. Through the previous analysis in this chapter, it can be concluded that the three algorithms can solve the basic RPC and have the same distribution law in typical cases. But for the data value of trend expression, as well as the optimization performance in the face of more complex, real-time data changes, and device values with nonequal ratios, a further comparative analysis is needed. The three algorithms compared in this paper are summarized in Table 7, and the common features in Table 1 are omitted.

After meeting the operational constraints of PVPS implanted in the control system, taking the actual operation condition of Foshan Hisense distributed PVPS as the input conditions shown in Figure 2, compare and analyze different distribution algorithms as follows. Among them, the upper limit values of RPC quantity ΔQΔQ under different distribution algorithms are compared, as shown in Figure 9.

Under the same operation condition, the higher the upper limit value of ΔQΔQ quantity is, the better the distribution and adjustment ability of the algorithm is. Therefore, under the same ΔQΔQ demand, the higher the upper limit value is, the larger the regulation margin of each device in PVPS is, the less PVPS resources needed are called, and the PVPS system will be relatively more stable.

Algorithms 1 and 2 are basically consistent in Figures 4 and 6, and there is no obvious difference for solving the demand of RPC. This is the reason many PVPS currently use Algorithm 1 with simple calculation and less data dimension to solve inverter cluster RPC. In the unchanged Night period, Algorithm 3 has a minimal margin advantage over algorithms 1 and 2, but it has a significant margin disadvantage at some times in the period of drastic changes, especially in the a.m. start and p.m. end periods. It shows that the imbalance of the system is serious during these drastic periods, and Algorithm 3 sacrifices the ΔQ margin to reduce the imbalance, which is the balance property.

The static capacity parameters of the topology in Figure 1 are shown in Table 3, and the differences between the unregulated and three RPD algorithms are simulated for the operation state shown in Figure 2 and Figures 10 and 11. The results show that only the transformers have a larger value during the night period, while inverters basically keep 0. This is due to the fact that the inverter stops generating power but the cable laid on low voltage of transformer absorbs small-capacity capacitive power from the grid through the transformer. However, the power is too small to affect the system at the night.

The value of planned ΔQΔQ in Figure 11 is uncertain over time. Observing the transformer and PV matrices, it can be found that the s_ps$_p$ of Algorithm 3 is basically smaller than Algorithm 1 and Algorithm 2 during the power generation period, while s_ps$_p$ of Algorithm 1 is larger than Algorithm 2. In addition, for the period when changes drastically at noon in PV matrix, it can be found that even if the RPC is increased by the device, s_p is still declining compared to the original s_p, indicating that a reasonable distribution algorithm can reduce the device imbalance and stabilize the system auxiliary while completing the RPC.

The $s_\varphi s_\varphi$ of Algorithm 3 changes violently when ΔQ is relatively small, and the $s_\varphi s_\varphi$ of Algorithm 1, 2, and 3 increase sequentially in the generation period, but it is still controlled within a reasonable range. For the transformer, when the power fluctuates greatly during the noon period, s_φ will exceed the original state, but it can be controlled below the original state in other power generation periods. In addition, Algorithm 1 and 2 will produce s_φ a sudden change at Day 6 noon, which is caused by the sharp power change and obvious demand of ΔQΔQ at the moment. However, Algorithm 3 will not have such an accident because s_φ is considered s_φ in the iteration.

The PV matrix distribution algorithm can significantly reduce $s_\varphi s_\varphi$ at the a.m. start and p.m. end time because the inverters use constant PF operation in the original state, so there is no dynamic method corresponding to the sudden change. The PV matrix is increased in most power generation periods after cluster control; however, s_φ still maintain a low level at most periods except the noon power generation time,

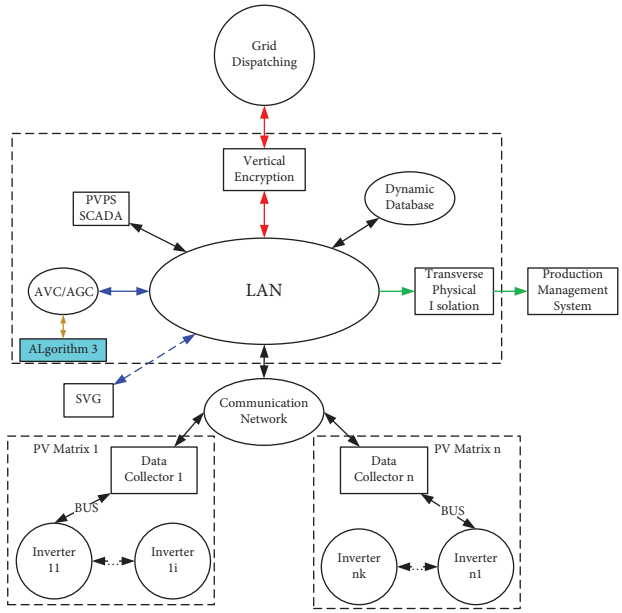

Figure 12: Schematic diagram of PVPS control system.

showing that a reasonable distribution algorithm can help to reduce the device imbalance while completing the RPC.

In general, the more data dimensions of parameter allocation, the better the comprehensive effect of optimization, and the greater the complexity of calculation. In actual operation, since the influence of length on voltage is greater than angle, s_ps$_p$ is more important than s_φ in selection.

4. Experiment

Algorithm 3 is used to test PVPS of the topology in Figure 1 in Foshan Hisense, and the device parameters are shown in Table 3. This paper adopts embedded development to realize the control logic in Figure 3 in Code Blocks with Linux system development environment. The control system is shown in Figure 12, which indicates that the work of this paper is a small part of PVPS. The PF comparison after experiment is shown in Figure 13, and by comparing the original conditions of the PVPS shown in Figure 2, it can be found that the PF fluctuation of PCC_{PV}PCC$_{PV}$ and inverter is obvious after the retrofit operation, which is the result of changing the fixed PF operation mode of the inverter group in the original station to the remote reactive power regulation mode. In this mode, the reactive power will not change with the active power generation. The overall reactive power output of the power station has relatively independent characteristics, and the reactive power value is relatively stable, thereby reducing the reactive power demand and suppressing the reactive power fluctuation at *PCC*PCC. The curve change of Q_{PCC}Q$_{PCC}$ in Figure 13 is the experimental proof expected by this theory.

The modified control system follows the demand of *PCC* to generate ΔQΔQ, to improve the PF of *PCC*PCC. It can be seen from the results that the steady-state PF value increases from 0.95 to 0.97, which significantly improves the power quality of the station and reduces the reactive power pressure

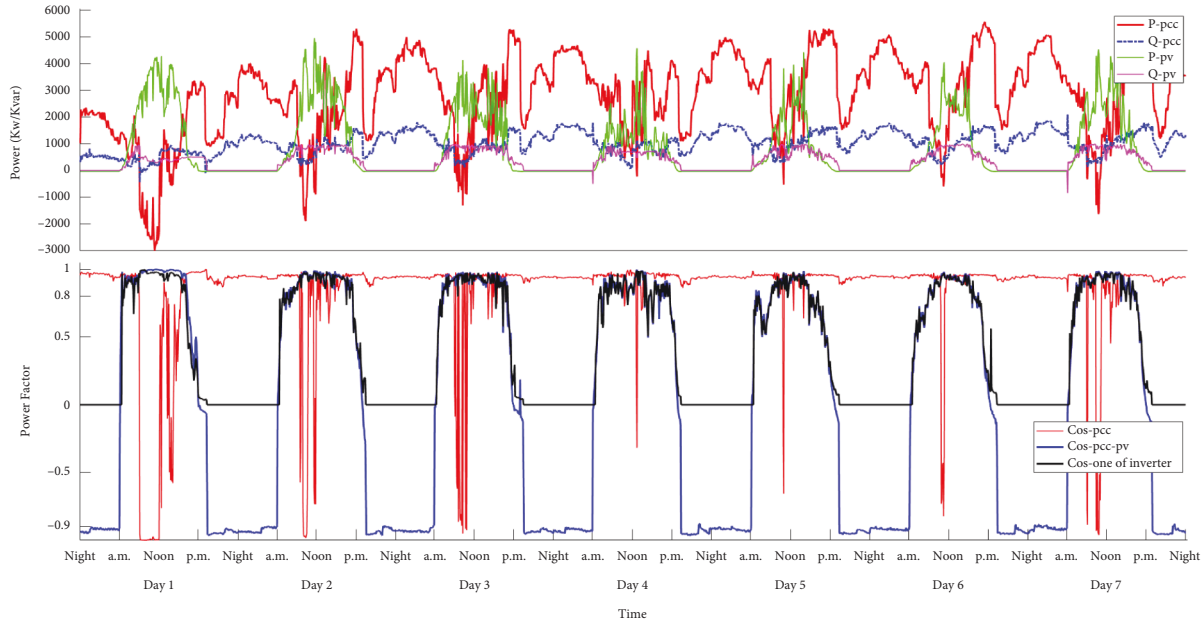

Figure 13: PF comparison diagram of PVPS under RPC.

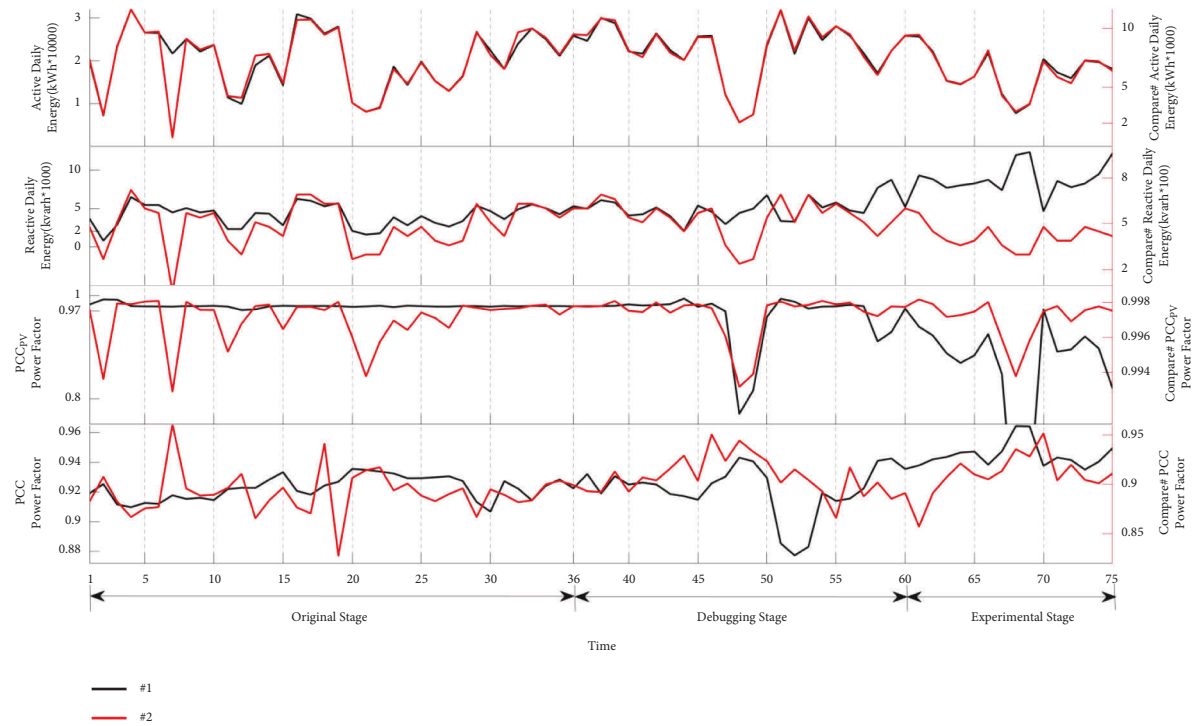

Figure 14: Control experiment daily diagram of PVPS under RPC.

of the grid. In this paper, some stable operation constraints such as overvoltage and undervoltage are set during the retrofit of control system, although, which is not described in detail, the retrofit process still includes many other steps besides the algorithm. Due to the factors such as bus voltage and device capacity, the compensation capacity cannot be continuously released. Therefore, the Q_{PV} Q_{PV} in Figure 13 shows a trapezoidal change. It is worth noting that since the operation experiment in Figure 13 is in summer and Figure 2 is in spring, the sampling environment in Figure 13 is faced with more sufficient illumination and drastic environmental changes, so the active power generation and PF change sharply during some periods. Figure 13 shows the effect after RPC, so it can be inferred that the power quality will be worse if RPC is not used.

In Foshan, one PVPS in the same area as Hisense was selected to conduct a control experiment. The operation results of 75 consecutive days were analyzed daily, as shown

in Figure 14. The cycle Figure 14 is divided into three consecutive stages, and the middle 36–60 days are the retrofit stage of the control system, which may not be representative. It can be seen from the figure that the active daily energy curve of the pilot power station has not deviated at any stage and has always maintained the same power generation law as the comparison power station, which verifies that the technical scheme in this paper does not cause any loss to the power generation. However, the reactive daily energy of the pilot PVPS has increased significantly, which has caused the PF of *PCC*PCC to decrease, while compensating the reactive power and improving the PF of *PCC*PCC. The whole process maintains the same operation law as Figure 13, and the experimental operation proves the economy and effectiveness of the technical route proposed in this paper.

5. Conclusion

In this paper, the influence of distributed PVPS on grid and the owner's power consumption quality during operation is analyzed, and the advantages of grid-connected inverter in RPC are explained. Three algorithms are designed by using different data dimensions to solve the problem of inverter group reactive power control, and the imbalance evaluation method is defined according to the system equilibrium target. In typical cases, the performance advantages of Algorithm 3 are obtained by comparison and analysis, but the data dimensions and calculation are also relatively complex.

Three algorithms are compared and analyzed by using one week's actual operation data of the power station, and compared with the fixed PF operation of the power generation device, cluster control can not only perform RPC but also reduce the imbalance of the system. The reactive power margin of Algorithm 3 proposed in this paper is low in some periods, which is due to sacrificing a certain margin to reduce the imbalance, but $s_p s_p$ is the lowest, and the $s_\varphi s_\varphi$ control does not undergo changes abruptly, so it has more advantages in a comprehensive performance.

Through the transformation of the control system to run Algorithm 3 in the actual power station, the experimental results show that the improvement of RPC through the inverter group is an effective way to improve power quality, and it is an important way of VVC in the future intelligent PVPS and high penetration of renewables grid.

In the future, consider voltage balance in the algorithm to further refine the control, and use the power generation device group control to adjust the frequency by active power to further improve the frequency characteristics of the grid. Among them, how to coordinate the voltage-frequency control is an important problem. In this paper, the experiment does not perform RPC when the inverter is not generating, but the inverter still has the ability of reactive power output at the moment, so it can consider how to use the nonpower generation period to support the power system economically. The refined management and control of renewables is an important part of constructing the new power system. According to the cluster control idea in this paper, the control, operation and maintenance, communication, and other fields of power stations can be expanded in the future to further promote digital intelligent power stations.

Data Availability

The data that support the findings of this study are available from the corresponding author upon reasonable request.

Conflicts of Interest

The authors declare that they have no conflicts of interest.

Acknowledgments

This work was supported by the National Basic Research Program of China (973 Program) for International S&T Cooperation Projects (2019YFE0118700).

References

[1] X. Liu, A. Aichhorn, L. Liu, and H. Li, "Coordinated control of distributed energy storage system with tap changer transformers for voltage rise mitigation under high photovoltaic penetration," *IEEE Transactions on Smart Grid*, vol. 3, no. 2, pp. 897–906, 2012.

[2] C. Good, "Environmental impact assessments of hybrid photovoltaic–thermal (PV/T) systems – a review," *Renewable and Sustainable Energy Reviews*, vol. 55, pp. 234–239, 2016.

[3] K. Mahmoud and M. M. Hussein, "Combined static VAR compensator and PV-inverter for regulating voltage in distribution systems," in *Proceedings of the 2017 Nineteenth International Middle East Power Systems Conference (MEPCON)*, IEEE, Cairo, Egypt, December 2017.

[4] S. Z. Chen, G. Xiong, G. Zhang et al., "An aerodynamics-based novel optimal power extraction strategy for offshore wind farms with central VSCs," *IEEE Access*, vol. 6, pp. 44351–44361, 2018.

[5] T.-T. Ku, C.-S. Chen, C.-H. Lin, C.-T. Hsu, and H.-J. Chuang, "Transformer management system for energy control of customer demand response and PV systems," *IEEE Transactions on Industry Applications*, vol. 55, no. 1, pp. 51–59, 2019.

[6] L. R. Vargas, S. E. Henrique, G. S. da Silva, and A. P. C. de Mello, "Local volt/var control strategy for smart grids using photovoltaic smart inverters," in *Proceedings of the 2019 IEEE PES Innovative Smart Grid Technologies Conference - Latin America (ISGT Latin America)*, IEEE, Gramado, Brazil, September 2019.

[7] S. Wang Chunjiang, J. Sun, J. Gong, and X. Zha, "Mechanism and damping strategy of interactive instability between," *Transactions of China Electrotechnical Society*, vol. 35, pp. 503–511, 2020.

[8] L. Jiao and J. Ma, "Research on reactive power characteristic of photovoltaic inverter," *Ningxia Electric Power*, vol. 1, no. 1, pp. 54–57, 2017.

[9] J. Junwei, M. Chao, Z. Qiyuan, and H. Qiang, "The principle of output reactive power of photovoltaic invertert," *Electronics World*, vol. 20, pp. 72–74, 2017.

[10] S. Zhu, *Research on Control Strategy of Active and Reactive Power for Photovoltaic Power Station in Energy Coordinated Control System*, North China Electric Power University, Beijing, China, 2015.

[11] J. Cheng, S. Li, Z. Wu, and J. Chen, "Analysis of power decoupling mechanism for droop control with virtual inductance in a microgrid," *Automation of Electric Power Systems*, vol. 36, no. 7, pp. 27–32, 2012.

[12] A. Dhaneria, "Grid connected PV system with reactive power compensation for the grid," in *Proceedings of the 2020 IEEE Power & Energy Society Innovative Smart Grid Technologies Conference (ISGT)*, Washington, D.C, USA, February 2020.

[13] D. Ibram and V. Gueorgiev, "Control of reactive power of a single-phase photovoltaic inverter," in *Proceedings of the 2020 12th Electrical Engineering Faculty Conference (BulEF)*, pp. 1–4, Varna, Bulgaria, September 2020.

[14] D. Fang, X. Guan, L. Lin, Y. Peng, D. Sun, and M. M. Hassan, "Edge intelligence based economic dispatch for virtual power plant in 5G internet of energy," *Computer Communications*, vol. 151, pp. 42–50, 2020.

[15] J. E. Quiroz, J. R. Matthew, L. Olga, and H. B. Raymond, "Communication requirements for hierarchical control of volt-VAr function for steady-state voltage," in *Proceedings of the 2017 IEEE Power & Energy Society Innovative Smart Grid Technologies Conference (ISGT)*, pp. 1–5, Washington, D.C., USA, April 2017.

[16] L. Zheng, R. P. Kandula, and D. Divan, "Soft-switching solid-state transformer with reduced conduction loss," *IEEE Transactions on Power Electronics*, vol. 36, no. 5, pp. 5236–5249, 2021.

[17] I. El-Samahy and E. El-Saadany, "The effect of DG on power quality in a deregulated environment," in *Proceedings of the IEEE Power Engineering Society General Meeting, 2005*, IEEE, San Francisco, CA, USA, June 2005.

[18] C. Ma, X. Da, Z. Yu, and Y. Zhang, "Voltage control strategy of SVG," *Electric Power Automation Equipment*, vol. 33, no. 3, pp. 96–99, 2013.

[19] W. Han, "Research and design for cascade SVG applied in photovoltaic power station," *Power Electronics*, vol. 51, no. 11, pp. 24–26, 2017.

[20] W. Liqiang, C. Bin, W. Qi, C. Yu, W. Haiyan, and X. Zhang, "Study on hardware-in-the-loop model and low voltage ride-through characteristics of photovoltaic power station," in *Proceedings of the 2019 4th IEEE Workshop on the Electronic Grid (eGRID)*, Xiamen, China, November 2019.

[21] M. Fajardo, J. Viola, J. M. Aller, and F. Quizhpi, "DC-link voltages balance method for single-phase NPC inverter operating with reactive power compensation," in *Proceedings of the 2019 IEEE 15th Brazilian Power Electronics Conference and 5th IEEE Southern Power Electronics Conference (COBEP/SPEC)*, Santos, Brazil, December 2019.

[22] P. Pachanapan, "The control of large scale grid-tied photovoltaic rooftop systems to avoid the power factor charge," in *Proceedings of the 2019 International Conference on Power, Energy and Innovations (ICPEI)*, pp. 24–27, Pattaya, Thailand, October 2019.

[23] V. Calderaro, G. Conio, V. Galdi, G. Massa, and A. Piccolo, "Optimal decentralized voltage control for distribution systems with inverter-based distributed generators," *IEEE Transactions on Power Systems*, vol. 29, no. 1, pp. 230–241, 2014.

[24] I. Kim, R. G. Harley, and R. Regassa, "The investigation of the maximum effect of the volt/var control of distributed generation on voltage regulation," in *Proceedings of the 2015 IEEE 42nd Photovoltaic Specialist Conference (PVSC)*, IEEE, New Orleans, LA, USA, June 2015.

[25] K. Mahmoud, N. Yorino, and A. Ahmed, "Optimal distributed generation allocation in distribution systems for loss minimization," *IEEE Transactions on Power Systems*, vol. 31, no. 2, pp. 960–969, 2016.

[26] Z. Chen, Y. Jianhua, W. Weizhou, and L. Fuchao, "A control strategy for static var generator to regulate voltage in distribution network under high penetration of photovoltaic," in *Proceedings of the 2018 2nd IEEE Conference on Energy Internet and Energy System Integration (EI2)*, IEEE, Beijing, China, October 2018.

[27] Y. Hu, W. Liu, X. Li, Z. Liu, W. Wang, and F. Liu, "A group division method for voltage control based on distributed photovoltaic scaled access to rural power grid," in *Proceedings of the 2020 5th Asia Conference on Power and Electrical Engineering (ACPEE)*, pp. 580–586, Chengdu, China, June 2020.

[28] X. Wu, H. Dai, Z. Xu, and Y. Lu, "Voltage control strategy of distribution network based on coordinated control of PV inverter and SVG," in *Proceedings of the 2019 IEEE 3rd International Electrical and Energy Conference (CIEEC)*, pp. 1907–1911, Beijing, China, September 2019.

[29] Z. Zhang, Y. Mishra, C. Dou, D. Yue, B. Zhang, and Y.-C. Tian, "Steady-state voltage regulation with reduced photovoltaic power curtailment," *IEEE Journal of Photovoltaics*, vol. 10, no. 6, pp. 1853–1863, 2020.

[30] M. Miranbeigi, P. Kandula, K. Kandasamy, and D. Divan, "Collaborative volt-VAR control using grid-connected PV inverters," in *Proceedings of the 2019 IEEE 10th International Symposium on Power Electronics for Distributed Generation Systems (PEDG)*, Xi'an, China, June 2019.

[31] S. Acharya, M. S. El Moursi, A. Al-Hinai, A. S. Al-Sumaiti, and H. H. Zeineldin, "A control strategy for voltage unbalance mitigation in an Islanded microgrid considering demand side management capability," *IEEE Transactions on Smart Grid*, vol. 10, no. 3, pp. 2558–2568, 2019.

[32] T. Pan, Y. Xiao, W. Lin, X. Jin, H. Luo, and J. Feng, "Research on reactive power and voltage equalization control strategy of photovoltaic inverter cluster," in *Proceedings of the 2021 IEEE 5th Conference on Energy Internet and Energy System Integration (EI2)*, pp. 220–224, Taiyuan, China, October 2021.